DOI: 10.1002/fuce.201100187

Water Flow in, Through, and Around the Gas Diffusion Layer

E. Gauthier[1], Q. Duan[2], T. Hellstern[1], J. Benziger[1]*

[1] Department of Chemical and Biological Engineering, Princeton University, Princeton, NJ 08544, USA
[2] College of Material Science and Engineering, State Key Laboratory for Modification of Chemical Fibers and Polymer Materials, Donghua University, Shanghai 201620, P. R. China

Received November 22, 2011; accepted August 10, 2012

Abstract

Liquid water produced in polymer electrolyte membrane fuel cells is transported from the cathode catalyst/membrane interface through the gas diffusion layer (GDL) to the gas flow channel. Liquid water travels both laterally (in the plane of GDL) and transversely through the largest pores of the porous GDL structure. Narrow apertures in the largest pores are the primary resistance to liquid water penetration. Carbon paper has limiting apertures ~20 μm in diameter and ~1 μm in length whereas carbon cloth has apertures ~100 μm in diameter and ~200 μm in length. After sufficient hydrostatic pressure is applied, water penetrates the limiting aperture and flows through the pore. The pressure required for water to flow through the pores is less than the pressure to penetrate the limiting aperture of the pores. Water moved laterally and directed through a small number of transverse pores. There is less resistance to lateral liquid water flow at the interface between the GDL and a solid surface than through the GDL. The results from these experiments suggest that water flow through the GDL is dominated by a small number of pores and most pores remain free of liquid water.

Keywords: Flow Through Pores, Gas Diffusion Layer, Water Penetration

1 Introduction

The gas diffusion layer (GDL) is an essential element of the electrodes in polymer electrolyte membrane (PEM) fuel cells. The GDL makes electrical contact with the catalyst layers to provide a larger area to carry the electronic current from the catalyst to the bipolar plates reducing the resistance for current flow. The GDL must be porous to permit the flow of reactant gas from the gas flow channel to the catalyst layer and flow of water from the catalyst layer to the gas flow channel. The GDL must be electrically conductive, but it is also desirable for it to be hydrophobic to keep liquid water from filling the pores and blocking gas flow to the catalyst layer. Figure 1 is a schematic of the flow paths for the reactant gases and liquid water in the GDL coupled with transport in the gas flow channels, proton transport in the PEM and electron transport through the external load.

There have been numerous studies characterizing the pore structure of GDL materials [1–12]. Gostick et al. have recently written a very comprehensive review of studies characterizing gas diffusion media [7]. Most studies of the GDL have focused on water flooding the GDL [1, 5, 8, 13–18]. Several investigators have reported saturation curves from imbibing and draining water into the gas diffusion media; this data has been analyzed to determine pore volumes, pore radii and the internal contact angle of GDL materials. Several studies have also examined the hysteresis between the imbibition and draining curves attributing it to contact angle hysteresis and geometrical effects [3, 4, 6, 10, 19].

Benziger et al. [20, 21] and coworkers introduced water penetration experiments to characterize GDL materials. Their results showed that carbon fiber GDL materials are hydrophobic and liquid water penetrates the largest pores. They suggested that liquid water only penetrates a few large pores and the smaller pores, that comprise the majority of the pore volume, remain free of liquid water and allow gas to be transported from the gas flow channel to the catalyst layer. Other researchers have employed NMR and neutron scattering imaging to confirm that liquid water penetrates only the largest pores [22–24]. The incipient water penetration results indicate that the tail of the pore size distribution is critical for controlling water transport.

[*] *Corresponding author, benziger@princeton.edu*

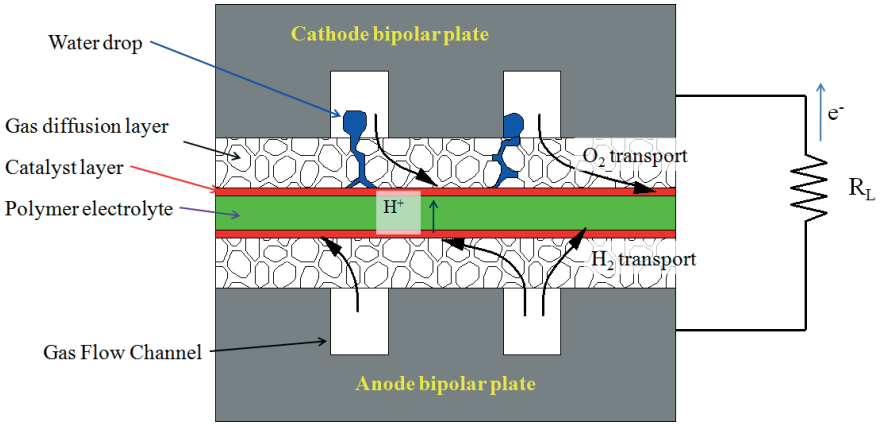

Fig. 1 Schematic of structure of flow channels and membrane electrode assembly showing the flow of liquid water from the cathode catalyst layer to the cathode gas flow channel.

Several studies have compared fuel cell performance with different GDL materials in efforts to correlate GDL pore and fuel cell performance [18, 25, 26]. A common focus is adding Teflon to the carbon fiber GDL materials to limit flooding [13, 15, 17, 27–29]. Other researchers have also considered the potential to control GDL saturation using a hydrophobic microporous layer (MPL) between the catalyst layer and the GDL [7, 30–34].

Water removal from PEM fuel cells depends on the coupled transport of water through the GDL and drop detachment in the gas flow channel. While the literature on flow channel design is extensive it seldom considers the coupled design of the GDL and the gas flow channel. Jiao and Zhao [14] and Lee et al. [35] developed models to show how larger and different shaped pores limit liquid water saturation of the GDL. Gerteisen et al. experimentally demonstrated that systematically perforating carbon paper with knowledge of the flow channel structure reduces water accumulation and results in increased limiting current densities of 8–22% [36]. Kimball et al. [37] created flow directing pores through the GDL. They reported the highest current density was achieved with a vertical flow channel, gas flow down, and the flow directing pore under the rib near the cathode gas inlet. By far the worst fuel cell performance was with a horizontal flow channel, cathode facing upward (with respect to gravity), and the pore directing pore under the channel near the cathode inlet. The efforts of all these studies suggest that the GDL and flow channels can be engineered to reduce the resistance to liquid water flow along certain pathways yielding less water saturation in the GDL and better fuel cell performance.

There have been a few previous studies that have examined the resistance to lateral flow [38–40]. However, as we will report in this paper it can be ambiguous as to whether the water flow is through the GDL or between the GDL–gasket interfaces. We shall quantify the resistance for liquid water flow through the different lateral flow paths. We shall also show that the lateral resistance to water flow changes over time, indicating slow dynamics of water penetration into some of the pores of the GDL cause partial flooding. Gostick et al. [7] suggested that the lateral transport gradient results in partial saturation and flooding of the cathode GDL. We will correlate our results with models of pore structures that explain the dynamics of partial saturation.

In this paper we report measurements of the resistances of transverse and lateral water flow associated with carbon paper and carbon cloth GDL materials, which we relate to pore structures of GDL materials. Carbon cloth has pores with nearly uniform diameter along their length. Carbon paper has wide pores with narrow necks. Liquid penetration is limited by the narrow pore necks, but after penetration the flow rate is controlled by the average pore diameter. Lastly, we will show that the resistance to lateral flow is substantially reduced at the interface between the GDL and a solid surface.

2 Experimental

2.1 Materials

The gas diffusion materials tested were purchased from Fuel Cell Earth LLC. Toray carbon paper materials (TGP-H-120) were obtained with treatments of 5, 20, and 40 wt.% Teflon and a thickness of 370 µm. Woven carbon cloth was supplied by Fuel Cell Earth with 0, 20 and 40 wt.% Teflon and a thickness of 380 µm. Figure 2 are micrographs of the two different GDL materials.

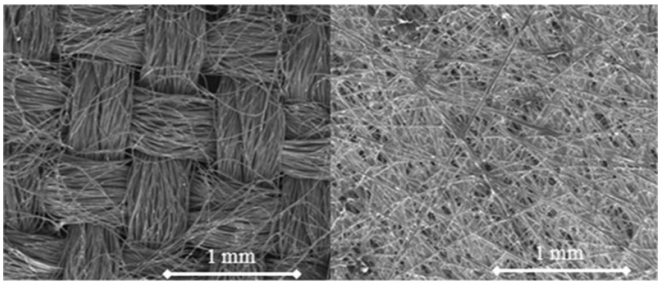

Fig. 2 Micrographs of carbon cloth and carbon paper GDL materials.

2.2 Transverse Transport Experiments

A cell similar to that used by Kimball et al. [21] was used to measure transverse liquid transport. A sample of GDL was sealed between two chambers. One of the chambers was filled with liquid water and connected to a water reservoir by a tygon tube; the other side was maintained at atmospheric pressure and allowed to drain directly to a beaker on an analytical balance (Ohaus Model AR0640). The piece of GDL exposed to water was 2.5 cm in diameter (total area of ~5 cm^2). GDL samples were stored in desiccators prior to testing. The water reservoir was placed on a lab jack that could

be raised or lowered relative to the GDL sample. The hydrostatic pressure of the liquid water was increased incrementally by 0.62 cm water (62 Pa) every 10 s until breakthrough was achieved. After breakthrough the flow rate was measured at fixed hydrostatic pressure interval for 100 s. Above breakthrough the hydrostatic pressure was increased in increments of 0.62 cm water and the flow rates were measured for 100 s. The GDL surface was visible through an acrylic plate, the number of drops forming on the surface of the GDL was recorded at each hydrostatic pressure. The pressure measurements are accurate to ±15 Pa. The standard deviations for the liquid flow rates were evaluated from ten measurements and were typically about ±10% for a given sample. Breakthrough pressures and flow rates were reproducible for a single GDL sample. However, there were larger differences between different samples taken from the same GDL material. We estimated the differences in values for breakthrough pressure between two different samples from the same GDL material were larger ±200 Pa for carbon cloth GDL and ±350 Pa for carbon paper GDL. We suggest that the larger difference between different samples the same material is the consequence of tail of the pore size distribution.

2.3 Lateral Transport Experiments

Lateral transport resistance was measured using an acrylic cell shown schematically in Figure 3. Water was forced through a lateral flow distance of 2.54 cm; the cross-section for flow was 0.47 cm wide × 0.038 cm high. A 2 L water reservoir pressurized with compressed air was connected to the cell. Pressurized water was pushed into an exposed are 0.47 cm in diameter on one side of a GDL strip, forced to flow laterally and then exit at atmospheric pressure from the other side of the GDL strip. The GDL was clamped between 300 μm thick silicon rubber gaskets, with holes for where the water entered and exited the GDL. The cell was assembled and six bolts tightened to 40 in-lbs. Water flow rate was determined by draining the cell into a beaker on an analytical balance (Ohaus Model AR0640). Two sets of measurements were made. One with the cell as described above with the silicon rubber gaskets. For the second set of measurements a thin coating of vacuum grease was applied to the faces of the silicon gaskets contacting the GDL material.

The pressure in the water reservoir was increased by increasing the regulator pressure on the compressed air. The pressure was increased in increments of 10 kPa from 50 to 300 kPa every 100 s. The liquid flow rates were determined from the change in mass of water collected over the 100 s collection interval. The lateral flow distance is 60 times greater than the transverse flow distance (2.5 cm *vs*. 0.04 cm and the pressures are 50 times greater for the lateral flow (300 kPa *vs*. 6 kPa for carbon paper) so the driving force for liquid flow, $\Delta P/L$, is approximately the same for the two different experiments.

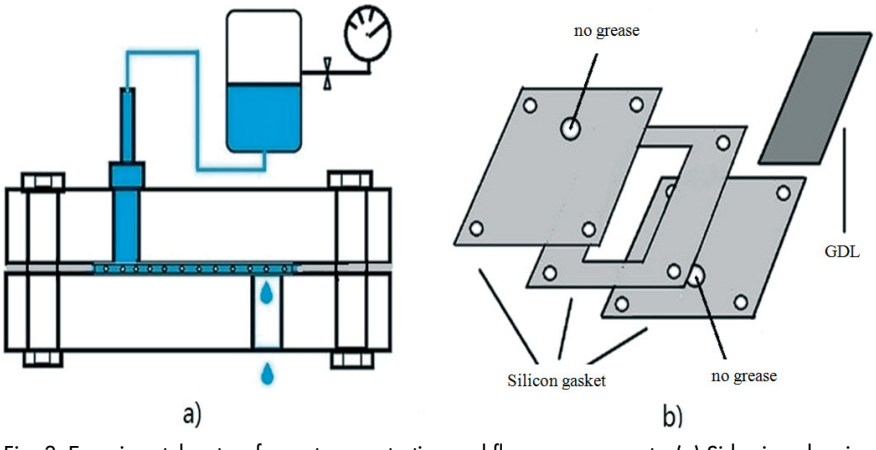

Fig. 3 Experimental system for water penetration and flow measurements. (a) Side view showing that an area of 0.17 cm^2 exposed to liquid water with a fixed hydrostatic pressure. The water traverses 2.54 cm of GDL material 1.5 cm wide and exits from the GDL. (b) 3-D view showing the positioning of the GDL material between two gaskets.

3 Results

3.1 Transverse Water Penetration

The water flow through carbon paper and carbon cloth GDL materials was measured as the pressure head was increased. The hydrostatic pressure head was set by positioning the water reservoir at a desired height above the permeation cell. The mass of water passing through the GDL was recorded every 10 s for 100 s. The pressure head was then increased. The breakthrough pressure was defined as the pressure when the first drop of water was collected on the balance. We could also see the GDL surface through a polycarbonate window and the formation of the breakthrough pressure corresponded to the formation of the first drop on the surface of the GDL sample.

After the initial breakthrough the hydrostatic pressure was increased by 62 Pa every 100 s and the accumulated liquid mass recorded. The surface of the GDL sample was viewed and the number of distinct liquid drops forming on the surface of the GDL was recorded. Each drop observed on the surface of the GDL was assumed to be associated with water penetration through a single pore in the GDL. Figure 4 shows the average mass flow rate as a function of hydrostatic pressure. A series of vertical lines are shown indicating the number of distinct drops seen on the surface of the GDL sample. The flow rates increase each time the number of drops increased. The flow rates also increased at some points where no new drop was observed. At those points one drop appeared to grow and detach at a faster rate than the others.

The hydrostatic pressure was increased until four to five drops were forming simultaneously and then the pressure was stepped down incrementally by steps of 62 Pa every 100 s and the flow rate was measured until the

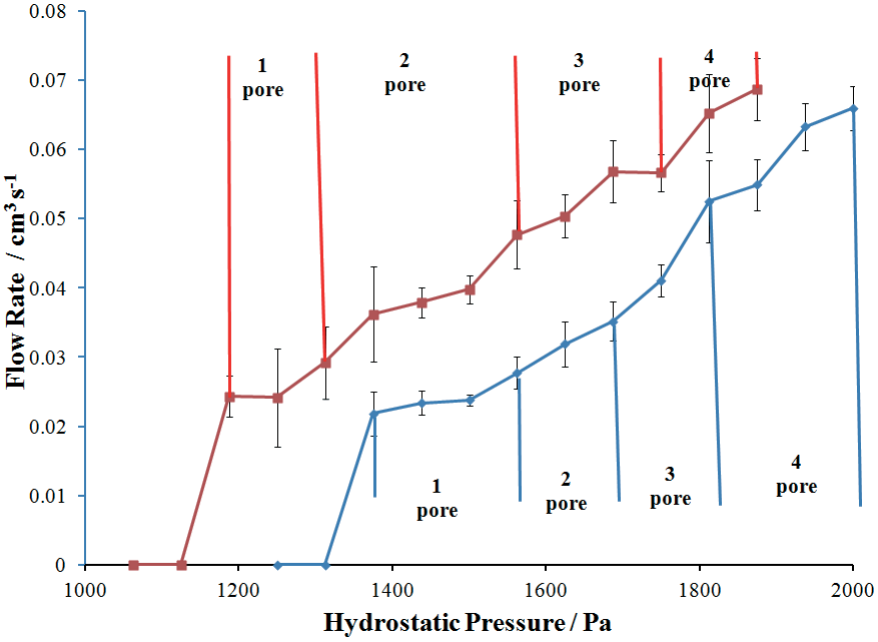

Fig. 4 Penetration of water through a carbon cloth GDL with 20 wt.% Teflon loading. Trial 1 (blue line) was for a sample initially fully dried. The vertical lines designate the number of distinct drops seen on the GDL surfaces during Trials 1 and 2. Trial 2 (red line) is water penetration for the same sample after initial water penetration from Trial 1.

flow of water ceased; the pressure when water flow ceased is referred to as the shutoff pressure. Figure 5 shows the flow rate for increasing pressure and decreasing pressure through a carbon cloth GDL with 20 wt.% Teflon loading. Flow commenced circa 1,000 Pa, corresponding to the breakthrough pressure. Flow did not shut off until the pressure was decreased to 250–300 Pa, corresponding to the shutoff pressure. The data in Figures 4 and 5 are for two different 20 wt.% Teflon loaded carbon cloth GDL samples. The results for breakthrough are similar, but the breakthrough and shutoff pressures show some variability reflecting slightly different pore sizes between samples.

The pressure required for liquid penetration through the GDL is much greater for carbon paper than for carbon cloth. Figure 6 is a bar graph that highlights the difference; penetration pressures for carbon paper with different Teflon loadings are five to six times greater than those for carbon cloth. After penetration through a single pore the flow rate for carbon cloth was two to three times greater than the single pore flow rate through carbon paper. The liquid flow rates at breakthrough were >0.025 g s^{-1}; that flow rate corresponds to a fuel cell current of 200 A. Current densities in PEM fuel cells are <2 A cm^{-2} which suggests that the water product from an area >10 cm^2 can be conducted through a single pore in the GDL. Table 1 summarizes the breakthrough pressure, the shutoff pressure, and the flow rate at the breakthrough pressure for different GDL materials. The shutoff pressure represents the minimum pressure differential between the cathode catalyst layer and the cathode gas flow channel to permit sustained (constant) water removal from the catalyst layer. If the pressure differential is below the shutoff pressure the hydrostatic pressure is insufficient to advance the contact line perimeter of the drop on outer surface of the GDL. The drop remains pinned when the Laplace pressure at the pore exit balances the sum of the hydrostatic and gravitation forces on the drop. Because the interfacial force pinning the drop is greater than the pressure required for water flow through the pore there is an abrupt drop in flow rate at the shutoff pressure. The flow rate at shutoff represents the minimum current required to have sustained steady liquid flow and a steady pressure differential between the catalyst layer and the gas flow channel. If the current is less than the flow rate at shutoff the liquid flow will stop and the pressure differential must build up to exceed the shutoff pressure for flow to recommence. The results in Table 1 suggest that in normal operation the pressure differential between the catalyst layer and the gas flow channel will fluctuate as liquid drops are removed from the surface of the

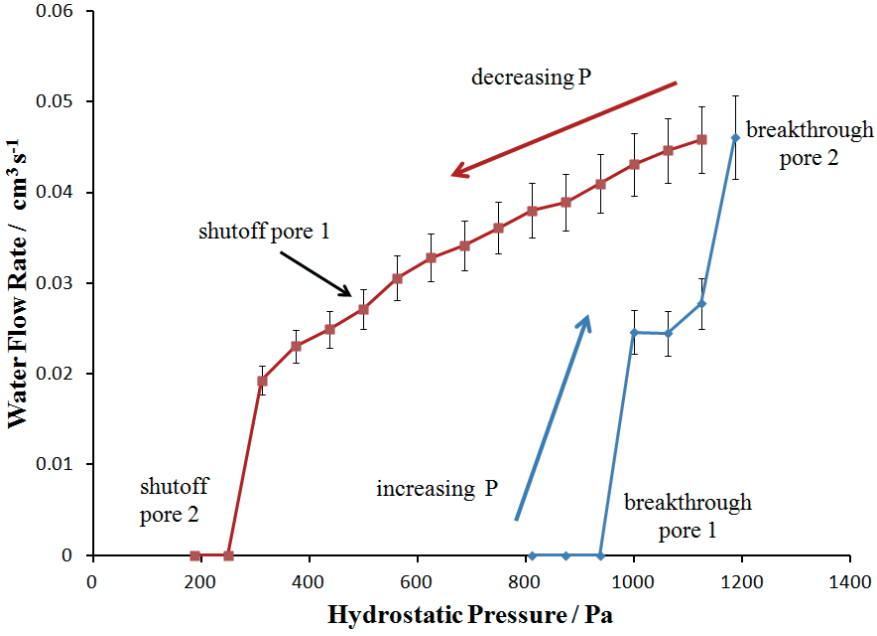

Fig. 5 Penetration and shut off of water flow through a carbon cloth GDL with 20 wt.% Teflon loading. The arrows designate the direction of pressure change.

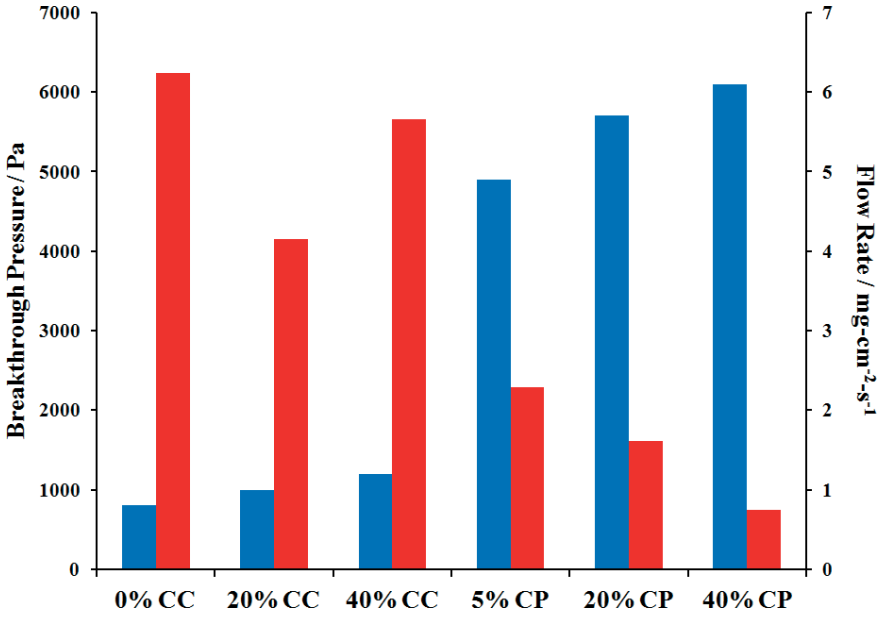

Fig. 6 Penetration pressures (blue bars) and flow rate at breakthrough (red bars) for transverse water transport for different GDL materials ##CP and ##CC stand for teflon loading wt.% carbon paper and carbon cloth, respectively.

Table 1 Penetration, shutoff, and flow through GDL materials.

GDL material	Penetration pressure (Pa)	Shutoff pressure (Pa)	Flow rate at initial penetration (mg cm^{-2} s^{-1})	Flow rate prior to shutoff (mg cm^{-2} s^{-1})
Carbon cloth	800	600	6.2	1.2
Carbon cloth + 20 wt.% Teflon	1,000	300	4.1	1.1
Carbon cloth + 40 wt.% Teflon	1,200	700	5.7	1.7
Carbon paper + 5 wt.% Teflon	4,900	2,900	2.3	1.1
Carbon paper + 20 wt.% Teflon	5,700	2,900	1.6	0.6
Carbon paper + 40 wt.% Teflon	6,100	4,200	0.7	0.7

GDL and the liquid pressure must increase to above the shut-off pressure for the next drop to form.

3.2 Lateral Flow

Lateral water transport through GDL materials was studied by forcing water in and out of point sources at opposite sides and at opposite ends of a strip of GDL material. The geometry is only approximately defined because the cross-section for flow in the GDL can spread perpendicular to the direction of flow (in Figure 3a this would be the direction pointing into the page). Trials were run with sample widths of 1, 1.5, and 2 cm; the fluxes increased by up to 20% between 1 and 2 cm wide samples. The samples were all ~300 µm thick, we did not have measurements of their compressed thickness. The results we report here are all for 1.5 cm wide strips.

A problem encountered with lateral flow measurements was sealing the sample between gaskets. Much larger flow rates were observed at the same hydrostatic pressure for sealing the GDL between hard rubber gaskets than between soft latex rubber gaskets. This indicated that the hard rubber gasket was not fully conforming to the topology of the GDL surface and the water could flow between the GDL and the gasket. To minimize water flow between the GDL and gasket a thin film of vacuum grease was spread on the gasket surface. The vacuum grease was easily deformed to match the surface topography of the GDL; water was forced to remain inside the GDL. Without the vacuum grease water preferred to flow between the GDL and the gasket surface.

A sharp penetration breakthrough for lateral water transport was not detected. No liquid flow was detected until the applied pressure was >50 kPa. After the first drop emerged the flow rate slowly increased during the 600 s dwell time at constant pressure. We cannot be certain that a small flow might have emerged at longer times; 50 kPa should be viewed as an upper bound on the lateral breakthrough pressure.

A significant difference between transverse and lateral flow is that the transport distance is much greater for lateral flow requiring a much larger pressure drop. We would expect a breakthrough pressure of ~5 kPa for the lateral flow, similar to the breakthrough for the transverse flow. However the flow rate at that pressure would be 100 times smaller for lateral flow making such an experiment impossible.

Figures 7 and 8 compare the lateral water flow rate through carbon paper and carbon cloth GDL materials as a function of the applied pressure. The flow rates were as averaged over 10 min. Flow rates are shown during four cycles of increasing and decreasing pressure. The first cycle shows a breakthrough pressure of ~50 kPa for both carbon paper and carbon cloth GDL. The breakthrough pressure appears to decrease with each cycle for carbon paper, while the breakthrough pressure appears to remain the same for each cycle with carbon cloth.

Carbon paper has a distinct hysteresis in the lateral water flow rate between increasing and decreasing pressure. The flow rate is greater with decreasing pressure than with increasing pressure. The flow rates increase with each cycle and the hysteresis diminishes with each cycle. Carbon cloth has a less pronounced hysteresis of flow rate with hydrostatic pressure than was observed with carbon paper. Carbon cloth also appears to have a non-vanishing breakthrough and shut-off pressure even after multiple cycles forcing water through the carbon cloth GDL.

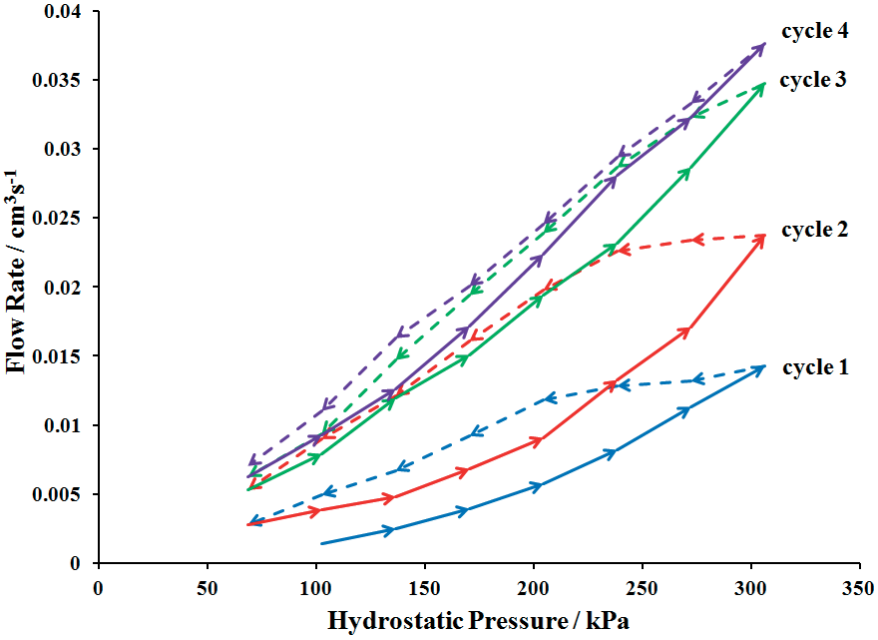

Fig. 7 Flow rate through carbon paper GDL with 5 wt.% Teflon loading as a function of increasing/decreasing hydrostatic pressure. The pressure was cycled four times from 68,000 to 306,000 Pa.

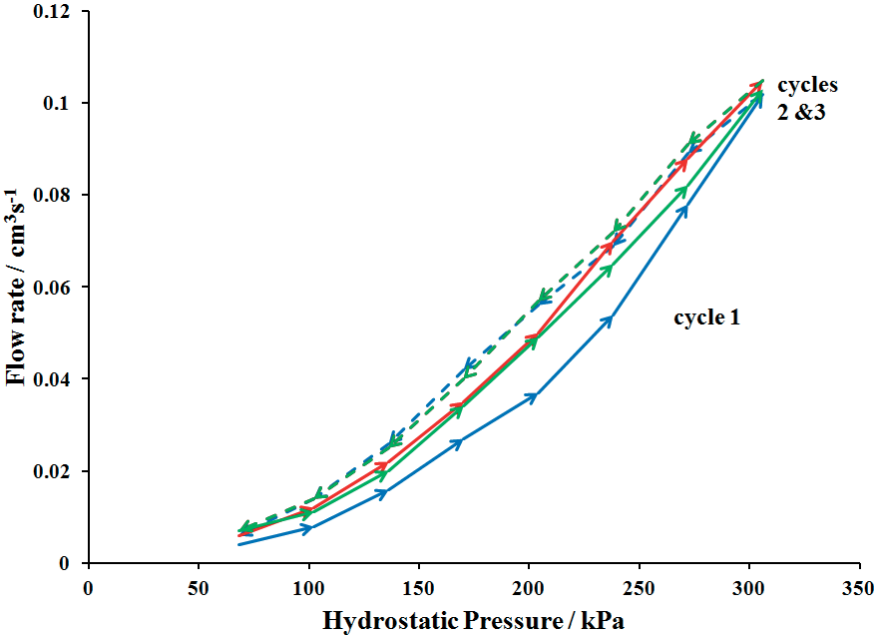

Fig. 8 Flow rate through carbon cloth GDL with 20 wt.% Teflon loading as a function of increasing/decreasing hydrostatic pressure. The pressure was cycled three times from 68,000 to 306,000 Pa.

Figure 9 is a comparison of water flow rate through Teflon treated carbon paper GDLs and water flow around Teflon treated carbon paper GDLs. Flow rates were taken after multiple cycles of forcing water through the lateral flow path so there was negligible hysteresis. The water flow is more than ten times greater when it flows between the gasket and GDL instead of being forced through the GDL.

The lateral flow rates as functions of the hydrostatic pressure were fit to a modified form of Darcy's law shown in Eq. (1), where $R_{\text{flow, lateral}}$ is the flow resistance, Q is the volumetric flow rate, μ is the viscosity, and $\Delta P/L$ is the hydrostatic pressure divided by the distance for transport. We use an effective flow resistance rather than permeability. Permeability is normally given as the product of porosity and tortuosity. However, the liquid water only accesses a fraction of the pore volume. The fraction of the pores penetrated by the liquid water depends on the applied pressure. Flow resistance is more convenient to use when considering series resistances as will be done later in this paper. The flow resistance is also dependent on the history of water penetration and flow through the GDL material.

$$Q = \frac{1}{\mu R_{\text{flow,lateral}}} \frac{\Delta P}{L} \tag{1}$$

Table 2 summarizes the lateral flow resistances through and around GDL materials. The values in Table 2 correspond to the least squares linear fit of Q *versus* ΔP values after cycling the pressure between 68 and 306 kPa four times. The flow resistance for flow between the GDL and the gasket are comparable to those previously reported by Feser et al. [38] The flow resistance for liquid flow through the GDL are much greater than those for liquid around the GDL. The flow resistances for liquid flow through the GDL are also more than ten times greater than gas phase permeabilities measured for GDL materials.

The flow rates at breakthrough for lateral transport were similar to those obtained for transverse transport, while the pressures for lateral flow are 100 times greater. The larger pressure drop for lateral flow is expected since the dis-

Table 2 Lateral flow resistances for GDL materials.

GDL material	R_{flow} (through) (m^{-4})	R_{flow} (around) (m^{-4})
Carbon paper + 5 wt.% Teflon	3.1E + 17	2.6E + 16
Carbon paper + 10 wt.% Teflon	3.3E + 17	2.6E + 16
Carbon paper + 20 wt.% Teflon	6.7E + 17	2.9E + 16
Carbon cloth	1.6E + 17	8.7E + 15
Carbon cloth + 20 wt.% Teflon	1.1E + 17	7.0E + 15
Carbon cloth + 40 wt.% Teflon	1.6E + 17	6.8E + 15

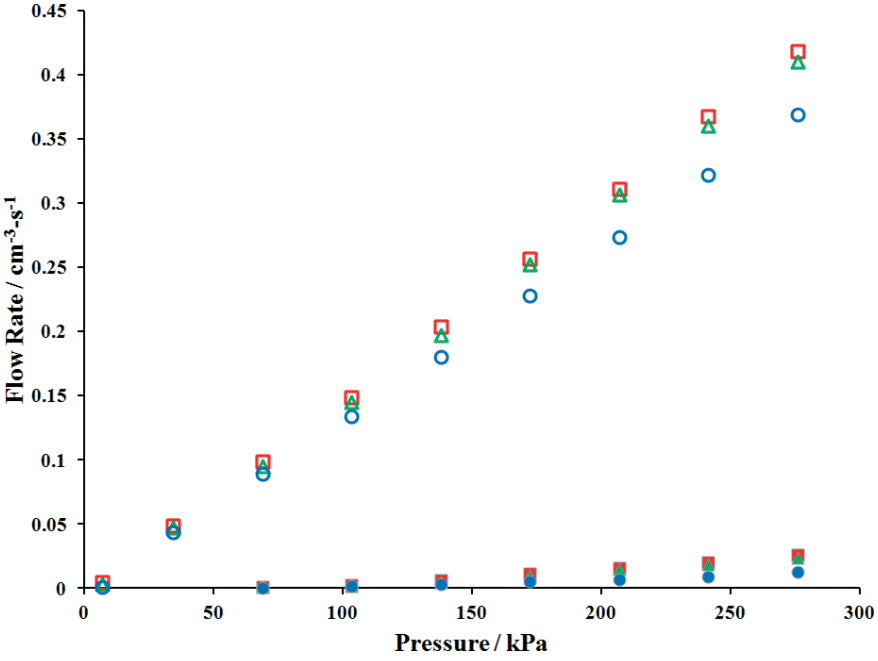

Fig. 9 Water flow through and around carbon paper GDL with different levels of Teflon loading. Solid symbols are flow through the GDL (vacuum grease applied at gasket-GDL interface). Open symbols are flow around the GDL (no grease applied). Red – 5% Teflon loading; green – 10% Teflon loading; blue – 20% Teflon loading.

tance for lateral transport through the GDL (~1 cm) is 100 times greater than the distance for transverse transport across the GDL (~0.01 cm). The flow rates for carbon cloth are three times greater than carbon paper, similar to the results seen for transverse flows reflecting greater porosity in the carbon cloth.

4 Discussion

Water is formed at the cathode catalyst layer in a fuel cell. At steady state there is liquid water present along most of the length of the cathode gas flow channel. Water is at vapor saturation in both the catalyst layer and in the cathode gas flow channel. There is negligible driving force for water vapor to be carried by diffusion. Liquid water must accumulate at the catalyst layer/GDL interface and build up a pressure to drive water transport from the catalyst layer to the gas flow channel. Water can flow laterally in the catalyst layer and at the GDL catalyst layer interface, and then be pushed transversely through pores in the GDL to the gas flow channel. The experiments presented here help identify the flow paths of least resistance for water transport.

4.1 Water Penetration Through the GDL

Gas diffusion media are complex heterogeneous materials. The surfaces have both chemical and topological heterogeneity. Chemical heterogeneity results from the addition of Teflon to coat the carbon fibers and make them more hydrophobic. Topological heterogeneity results from the void spaces between fibers resulting in a combination of liquid/solid and liquid/vapor interfaces within the porous GDL network.

Gas diffusion media made from carbon fibers are hydrophobic. The macroscopic contact angle of water with individual carbon fibers are approximately 90°; the contact angle of water with Teflon is 105° and the contact angle of water with carbon cloth and carbon paper with and without Teflon treatments is >150°. [20, 41–45]. Recent work by Gauthier et al. showed that the topological roughness of GDL surfaces greatly increases the hydrophobicity of the surface and can result in dynamic superhydrophobicity. The work of Gauthier indicated that surface topology has a much greater effect on the wetting of GDL surfaces than the addition of Teflon. We will employ a simplified pore model with an effective solid/liquid contact angle equal to that of Teflon. The results from Gauthier et al. [19] and also the work of Das et al. [45] indicate there could be larger or smaller effective contact angles. The quantitative analysis of pore diameters depends on the water/pore surface contact angle. Predictions should be viewed as semiquantitative, the trends predicted should be correct, but the absolute values could be off by a factor of 2–3.

Liquid water prefers to be outside the GDL. For water to penetrate the GDL pressure must be applied; only when the hydrostatic pressure is sufficient to overcome the surface energy between liquid water and the GDL pore openings can water penetrate into the pores of the GDL. At breakthrough the hydrostatic pressure must be sufficient to push water through each neck or aperture in the path that the water traverses.

The minimum pressure required to push liquid water through the GDL corresponds to water passing through the smallest aperture of the largest pore. Figure 10 schematically illustrates four pores (A–D) in the GDL. Larger scale topology of the pores is reflected in different pore size openings; smaller scale roughness of the walls of the pores would be expected to result in an advancing contact angle of water with the pore walls of ~150°. When there is no applied hydrostatic pressure liquid water is excluded from all pores of the GDL. As the hydrostatic pressure of water increases the water will penetrate into the pores of the GDL. Previous analyses of water penetration have generally assumed uniform pores in the GDL with complex connectivity [20–24]. Figure 10 presents an alternative type of pore structure where the pores have variable diameters along their length. We neglect here differences in pore length and connectivity of pores. These factors will be introduced later. Water penetration and even-

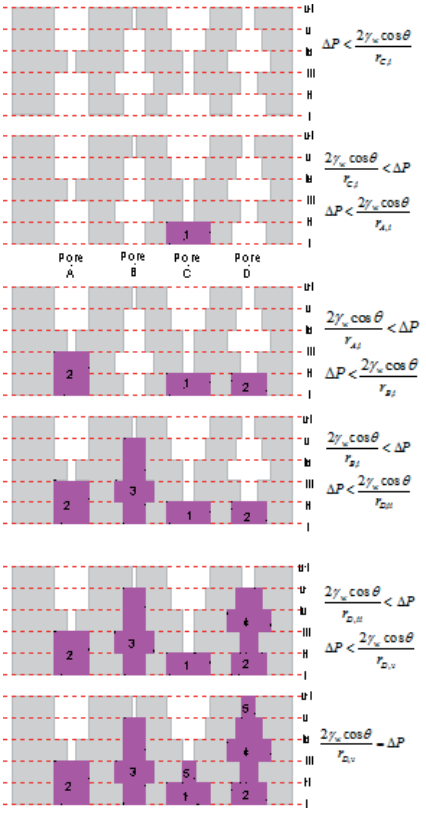

Fig. 10 Sequential filling of pores up to liquid breakthrough. The numbers correspond to the sequence of water penetration described in the text. Stage 5 corresponds to liquid breakthrough and the commencement of steady liquid water flow through the GDL.

tual flow through a pore can be broken down into a sequence of stages.

Stage 1: When the hydrostatic pressure is increased, water will first enter the pore with the largest entry aperture (pore C). The hydrostatic pressure for water to enter pore C is given by the Young–Laplace equation [Eq. (2)].

$$\Delta P_{C,i} = \frac{2\gamma_w \cos\theta}{r_{C,i}} \tag{2}$$

Stage 2: Water will only enter pore C up to level ii until the pressure is increased to $\Delta P_{A,i} = 2\gamma_w \cos\theta / r_{A,i}$ and then water will penetrate into the entries of pores A and D. Pore A will fill to level iii, pore C will remain pinned at level ii and pore D will fill to level ii.

Stage 3: Increasing the pressure to $\Delta P_{B,i} = 2\gamma_w \cos\theta / r_{B,i}$ will allow water to fill pore B to level v, while the levels in all the other pores remain pinned because of the contact line forces at the narrowed pore apertures.

Stage 4: Increasing the pressure to $\Delta P_{D,ii} = 2\gamma_w \cos\theta / r_{D,ii}$ will allow water to penetrate further into pore D up to level v. The liquid levels in all the other pores remain pinned.

Stage 5: Increasing the pressure to $\Delta P_{C,ii} = \Delta P_{D,v} = 2\gamma_w \cos\theta / r_{C,ii} = 2\gamma_w \cos\theta / r_{D,v}$ will permit water to flow into pores C and D. The level in pore C will rise to between levels iii and iv, while the water in pore D breaks through to exit into the gas flow channel. After water breaks through in pore D the resistance to flow through pore D drops and water flows through pore D with the water levels in pores A, B, and C staying fixed.

The liquid flow rate through pore D at breakthrough can be found by taking the sum of the resistances through each section of the pore. A simplifying assumption is that the pressure drop through each section is given by the Hagen–Poiseuille equation [46]. Summing up the contributions to the overall pressure drop gives Eq. (3), where t_i is the length of each section along the pore and r_i is the radius of the aperture of each section.

$$\frac{\Delta P}{t_{GDL}} = \sum\left(\frac{\Delta P_i}{t_i}\right) = Q\mu_w\left(\frac{8}{\pi}\right)\sum\frac{1}{r_i^4} \tag{3}$$

Additional water will only flow into pores A–C if the pressure is raised above $\Delta P_{D,v}$. With increasing hydrostatic pressure pore C would be the next pore to fill and breakthrough so liquid would flow through pores C and D. As the pressure was increased further pore B would fill with liquid to level v, followed by penetration through pore A, and lastly, water will penetrate pore B.

If the hydrostatic pressure is decreased flow will shut off in order B, D, A, and C. Flow through a pore shuts off when the hydrostatic pressure is no longer sufficient for water to overcome the surface tension holding the drop to the pore exit. The shutoff pressure is found by using the radius of the pore exit in the Young–Laplace equation. The final shutoff pressure when all liquid flow ceases is $\Delta P_{D,v} = 2\gamma_w \cos\theta / r_{D,v}$.

The pore filling and breakthrough sequence illustrated in Figure 10 is applicable to both lateral and transverse flow in and through the GDL. This model can assist in explaining the hystereses observed when cycling the hydrostatic pressure. Suppose the pressure is increased to $\Delta P_{D,v}$ so only Pore D allowed flow; if the pressure were then decreased below $\Delta P_{D,v}$ liquid flow would shut off. Flow would recommence if the pressure were again raised to $\Delta P_{D,v}$. But as the pressure is increased the liquid front in Pore C will advance toward level iv. After cycling the pressure up and down the liquid front in Pore C will eventually reach level iv and liquid will flow through both Pore C and Pore D. This corresponds to the cycle dependent hysteresis seen with carbon paper shown in Figure 7.

4.2 Transverse Water Flow and Pore Structure

Transverse water flow in all the tested GDL materials requires an applied hydrostatic pressure, clearly demonstrating that the GDL materials are hydrophobic. Water seeks the path of least resistance to flow through the GDL, which will be the pore with the largest restricting aperture (in mathematical terms this corresponds to the maximum of the minimum pore aperture, which was Pore D in Figure 10). From the pressures and flow rates at breakthrough and shutoff the lim-

iting aperture for water flow, the radius of the pore exit and the effective length of the limiting aperture can be determined. The radius of the limiting aperture for water breakthrough is found applying the Young–Laplace equation to the breakthrough pressure [Eq. (4)].

$$r_{\text{breakthrough}} = \frac{2\gamma_w \cos\theta}{\Delta P_{\text{breakthrough}}} \quad (4)$$

The limiting apertures for the different GDL materials are listed in Table 3 using the breakthrough pressure for the first drop and assuming a contact angle (θ) of water with Teflon coated fibers of 110° [44, 47, 48]. The breakthrough radii are ~15–20 μm for carbon paper GDL and ~80–120 μm for carbon cloth. The breakthrough pressure for drops 2–5 differs from drop 1 by ~10% indicating that the restricting pore radii differ by ~10%. The results in Figure 4 and Table 1 indicate that the breakthrough pressure decreased after initial wetting of the GDL. This could mean that the pore aperture had increased or the effective contact angle of water with the pore surface decreased. We suggest that a small amount of residual water remained attached in the porous GDL and this water reduced the apparent contact angle of water with the GDL surface.

The breakthrough pore radii depend on the contact angle between water and the pore walls. The estimates provided in Table 3 assume smooth pore walls with a contact angle of 110°. Because of the irregular topology of the pores – they are not cylindrical, they are not straight, they are not smooth, and they may have variable chemical composition – the pore radii should be viewed as semiquantitative. These model values should be viewed as effective radii for transport modeling purposes.

The radius of the pore exit is obtained from the pressure at which water flow through the GDL shuts off. Pore exit radii are given in Table 3; pore exit radii are typically 20–50% larger than the breakthrough radii. These results suggest that the limiting aperture is not at the pore exit.

We calculated the expected water flow rate through a single cylindrical pore with radii equal to the breakthrough radii at the breakthrough pressure. The calculated flow rate for carbon paper was approximately 100 times less than the measured flow rate, indicating that the average pore radius for carbon paper is significantly larger than the minimum pore aperture. Assuming that the pressure drop for flow occurs primarily across the limiting pore aperture, the length of the constriction can be determined from the Hagen–Poiseuille flow law [Eq. (5)].

$$t_{\text{aperture}} = \frac{\pi\left(\Delta P_{\text{breakthrough}}\right)\left(r^4_{\text{breakthrough}}\right)}{8Q_{\text{breakthrough}}\mu_w} \quad (5)$$

The effective lengths of the apertures for carbon paper are 1–2 μm, representing only a small fraction of the overall GDL thickness; values of the aperture lengths are given in Table 3. In contrast the effective lengths for carbon cloth are comparable to the thickness of the GDL. *Carbon cloth has a set of nearly uniform pores that traverse the GDL, but carbon paper has pores with small apertures, which limit the flow of water.* The pores in the carbon cloth can be identified in Figure 1, they are the openings at the intersections of the fiber bundles. Carbon paper GDL has no long range ordering of the fibers which is why it has smaller shorter apertures for flow.

The flow resistance at breakthrough through a single pore is given by Eq. (6); this resistance corresponds to flow through the limiting aperture of a single pore, and is evaluated by combining Eqs. (1) and (5).

$$R_{\text{flow,breakthrough}} = \frac{8}{\pi r^4_{\text{breakthrough}}}\left(\frac{t_{\text{aperture}}}{L}\right) \quad (6)$$

For carbon paper with $r_{\text{breakthrough}} = 10$ μm and $L/t_{\text{aperture}} = 100$ the resistance to flow is 2.6×10^{17} m^{-4}; and for carbon cloth with $r_{\text{breakthrough}} = 50$ μm and $L/t_{\text{aperture}} = 1$ the resistance to flow is 2.2×10^{16} m^{-4}. The transverse flow resistances based on Poiseuille flow are in good agreement with the experimental lateral flow resistances measured. This indicates that both lateral and transverse flow in GDL is dominated by limiting apertures along a single flow path.

Transverse water flow is controlled by only a few large pores in the GDL. Measurements of the saturation curves for GDL materials look at the pore size distribution and provide average pore sizes and pore volume. It is the tail of the pore size distribution that determines liquid water flow, and saturation measurements are not very sensitive to characterize the tail of the distribution. Water penetration measurements provide a better characterization of the pores relevant to liquid water flow. Porosity determined by saturation measurements is important to determine the gas flow rates from the gas flow channel to the catalyst layer.

4.3 Lateral Flow

The lateral flow experiments involved longer distance than the transverse flow experiments. In the case of the lateral flow the overall length of the pores is increased to ~25,000 μm, compared to ~400 μm for transverse flow through the GDL. The longer lateral flow path will introduce multiple constricting apertures and branches. The lateral and transverse flow resistances, given by the ratio of water flow rate to the pressure gradient ($QL/\Delta P$), were nearly the same, suggesting that the GDL materials are isotropic for water flow.

Table 3 Characteristic pore dimensions of GDL materials.

GDL material	$r_{\text{breakthrough}}$ (μm)	r_{exit} (μm)	t_{aperture} (μm)
Carbon cloth	120	180	410
Carbon cloth + 20 wt.% Teflon	99	320	320
Carbon cloth + 40 wt.% Teflon	79	140	120
Carbon paper + 5 wt.% Teflon	20	34	1.1
Carbon paper + 20 wt.% Teflon	17	34	1.1
Carbon paper + 40 wt.% Teflon	16	23	1.6

The hystereses in flow rate between increasing pressure and decreasing pressure seen in Figures 7 and 8 indicate that water does not find the path of least resistance on its first penetration through the GDL. A constricting pore can inhibit flow through pores with large average diameter and force water to flow through a pore with smaller average diameter, as is illustrated in Figure 11. Flow commences when the pressure exceeds the breakthrough pressure for Pore B. Most of Pore A fills with water but there is no flow through Pore A due to the constriction. When the pressure is increased above the breakthrough pressure for Pore A water will flow through both pores, but the flow resistance is smaller through Pore A. When the pressure is decreased below the breakthrough pressure for Pore A the limiting aperture is filled with liquid that permits water flow to continue.

The flow hysteresis was smaller for carbon cloth than carbon paper. It is evident from the micrograph in Figure 1 that the alignment of the carbon fibers in the woven carbon cloth will produce a more uniform pore radius along the length of the pores. Carbon cloth is more like Pore B in Figure 11, it has more uniform pores that display small hystereses. Carbon paper is like Pore A with small apertures in large pores that limit penetration. Penetration requires a higher pressure but the flow resistance is reduced after breakthrough.

The lateral flow resistance was substantially reduced at the GDL/gasket interface compared to flow through the GDL. We suggest that the topological mismatch of the GDL surface and the flat gasket surface resulted in larger effective pores through which the water was transported. Topographical mismatches at interfaces can provide greater volumes to facilitate lateral flows.

4.4 Lateral Water Collection – Coupling Lateral and Transverse Flow

The transverse liquid water flow through a single GDL pore is equivalent to an integrated current of 50–200 A, corresponding to a fuel cell area of >10 cm^2. Provided the lateral flow resistance for water transport is less than the transverse breakthrough resistance *the water product from the fuel cell could be directed to flow through a small number of pores in the GDL.*

Kimball et al. [21] and McCain et al. [16, 49] have shown that the water exits the GDL into the cathode gas flow channel in a few distinction locations. The water must have moved laterally in the catalyst layer or the GDL to be directed through a few specific pores. *Over how large an area is the water collected and directed through a transverse pore of the GDL?* Figure 12 illustrates water collection in two dimensions. The GDL is represented as a series of transverse pores that connect the catalyst layer to the gas flow channel. At the interface between the catalyst layer and the GDL there are a series of lateral pores (either through the GDL or at the GDL/catalyst layer interface). Water flow collected over a distance L will be directed through a single transverse pore provided that the sum of the pressure drop due to lateral flow to the entry point of the transverse pore plus the pressure drop due to flow through the transverse pore is less than the pressure required to penetrate a nearby pore.

$$(\Delta P)_{\text{lateral}} + (\Delta P)_{\text{transverse}} < (\Delta P)_{\text{penetration}}$$

$$\mu_w Q\left(\frac{8}{\pi r^4_{\text{breakthrough}}}\right) t_{\text{aperture}} + \mu_w Q R_{\text{flow,lateral}} L < \frac{2\gamma\cos\theta}{r_{\text{breakthrough}}} \quad (7)$$

The collection distance is then given by Eq. (8).

$$L < \frac{1}{R_{\text{flow,lateral}} r_{\text{breakthrough}}}\left[\frac{2\gamma\cos\theta}{\mu_w Q} - \frac{8 t_{\text{aperture}}}{\pi r^3_{\text{breakthrough}}}\right] \quad (8)$$

The liquid flow rate is equal to the current density (j) and collection area (L^2) divided by twice Faraday's constant (F), $Q = jL^2/2F$. Estimates of the collection distance for a current density of 1 A cm^{-2} are summarized in Table 4 for different scenarios of carbon paper or carbon cloth and the limiting flow resistance either through or around the GDL. The collection lengths are >5 cm for all the scenarios presented in

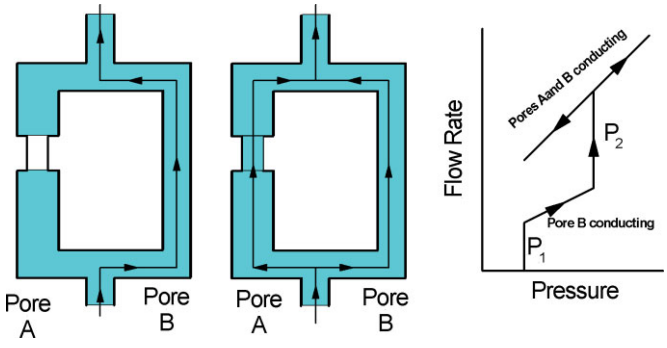

Fig. 11 Flow through parallel pores in the GDL. Initial water breakthrough is through the pore with the smaller mean diameter that has a larger limiting aperture. If the hydrostatic pressure is increased the pore with the larger mean diameter is opened up for flow and greater flow is permitted.

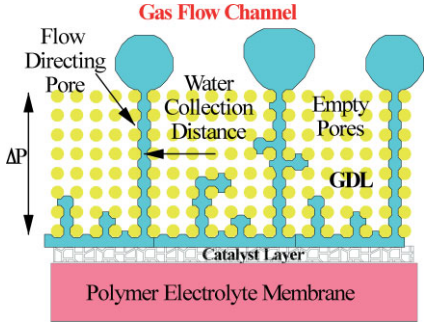

Fig. 12 Water is forced through pores spaced at a distance where the pressure drop from the sum of the lateral and transverse flow is less than the pressure required to penetrate a pore. The pores colored in blue are those filled with water transporting water from the catalyst layer to the gas flow channel. The pores colored white are not penetrated with water and remain open to transport oxygen from the gas flow channel to the catalyst layer.

Table 4 Liquid collection distances.

GDL material	$r_{breakthrough}$ (μm)	$t_{aperture}$ (μm)	$R_{flow,lateral}$ (m^{-4})	Collection distance L (cm)
Carbon cloth + 20 wt.% Teflon (though GDL)	99	320	1.1E + 17	5.4
Carbon paper + 20 wt.% Teflon (through GDL)	17	1.1	6.7E + 17	5.3
Carbon cloth + 20 wt.% Teflon (around GDL)	99	320	7.0E + 15	13
Carbon paper + 20 wt.% Teflon (around GDL)	17	1.1	2.9E + 16	15

Table 4, which is consistent with the experimental observations of only a few locations where drops emerge from the GDL.

The collection area increases with decreasing lateral flow resistance and decreasing breakthrough pore radius. We did not report experimental results here on the effect of an MPLs applied to the GDL. In previous work Benziger et al. [20] showed that the MPL layer had smaller pores than the carbon fiber GDLs. The smaller pores of the MPL should increase the size of the collection area according to Eq. (8). The analysis presented here quantifies the suggestion of Gostick et al. [7] that lateral flow at the MPL/GDL interface is important to the water collection mechanism.

The lateral collection area will be influenced by a variety of factors not included in the simple model presented above; some of the complexities are listed below.

(i) Compression of the GDL during fuel cell assembly due to alternating land and flow channel regions will impact lateral flow resistance and directionality.
(ii) Heated compression of the membrane electrode assembly will alter the interfaces between the catalyst layer/MPL/GDL which will impact the lateral flow resistance.
(iii) Addition of Teflon and Nafion as binders to the MPL and catalyst layers will alter pore constrictions of both transverse and lateral pores.
(iv) Membrane swelling from water sorption will alter the compression on the GDL.

We have not attempted to quantify how the lateral and transverse flow resistances are altered by the factors listed above. However, $R_{flow,lateral}$ for the catalyst layer GDL interface should be bounded by the resistance to flow through the GDL and the resistance to flow between the GDL and a solid gasket. The lower limits in Table 4 are ~5 cm, which agree with the results of Kimball et al. that found a single large pore in a carbon cloth GDL could collect the water from 6 cm^2.

4.5 Implications for Fuel Cell Design

Kimball et al. demonstrated with small fuel cells (<10 cm^2) that water flow through the GDL could be directed through a single pore. Flow directing pores could be located under the channel or the ribs of the bipolar plate. The results presented here suggest flow directing pores could be should be spaced <5 cm apart. In principle the GDL could be modified with a network of flow directing pores to direct water to exit into the cathode gas flow channel to improve both membrane humidification and liquid water removal. For example, in a parallel flow channel arrangement non-uniformity of water distribution between channels can result in gas flow bypass through channels with low content. Flow directing pores could be punched through the MPL and GDL to provide uniform water distribution flowing from the catalyst layer into the gas flow channels of the bipolar plate as illustrated in Figure 13. The uniform distribution of water would reduce the problem of having flooded and dry channels from randomly distributed water.

Previous work with the GDL has focused on hydrophobic treatments with Teflon and adding an MPL to minimize water intrusion into the GDL [7, 13, 15, 17, 27–34]. The work of Kimball et al. [37] coupled with the GDL characterization presented here show that the flow of water from the catalyst layer through the GDL is a component of the fuel cell design. Pores may be created in a hydrophobic GDL material that can minimize flooding, improve membrane humidification, and facilitate water removal. A bimodal pore size distribution is most desirable. There should be large lateral pores and a few large transverse pores that permit liquid water to be collected over a large area and directed through the GDL. There should be an abundance of small hydrophobic transverse pores that exclude water and allow gas to be transported from the gas flow channel to the catalyst layer. The most precise control occurs when the small pores are as small as possible, and there are only a select number of large pores. Of course, with these large pores the impact on electrical conduction pathways must also be considered [50, 51].

The essential message from the results and analysis presented here is that GDL can be designed to direct water flow into the cathode gas flow channel to mitigate problems associated with flooding and humidification in PEM fuel cells.

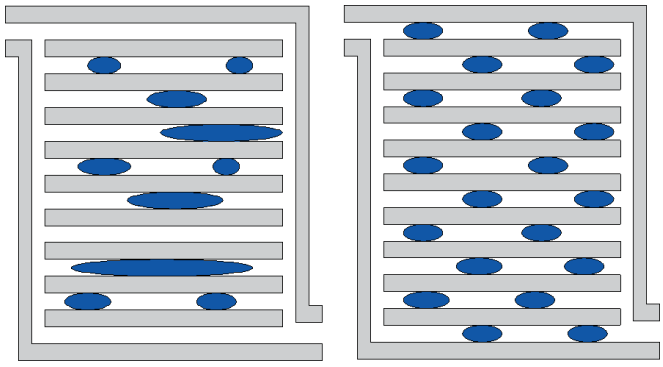

Fig. 13 Flow directing pore network in the GDL to provide uniform liquid distribution in parallel flow channels of the bipolar plate. In the flow channel at the left the pores are randomly distributed that results in a random distribution of water in the flow channels. In the flow channels at the right a set of flow directing pores has been uniformly spaces to give uniform liquid distribution in the flow channels.

5 Conclusion

Water flow in, through and around carbon paper and carbon cloth GDL materials has been studied. The GDL materials are hydrophobic and pressure must be applied to force water to intrude the pores of the GDL. Water flows through the path of least resistance.

(i) Transverse water flow commences when the applied hydrostatic pressure exceeds the Laplace pressure associated with the smallest aperture of the largest pore in the GDL. The pressure drop for water flow through the pore is less than the pressure required for penetration of the smallest aperture. Water sequentially penetrates smaller pores as the hydrostatic pressure is increased.

(ii) The water flow rate at penetration through the largest pore in carbon paper is 100 times greater than predicted for a uniform diameter cylindrical pore with radius equal to the penetration aperture; the transverse pores in carbon paper have large mean diameters with penetration limited by small aperture necks.

(iii) The water flow rate at penetration through the largest pore in carbon cloth is approximately equal to that predicted for a uniform diameter cylindrical pore with radius equal to the penetration aperture; the transverse pores in carbon cloth have uniform diameters.

(iv) The resistance to lateral water flow through the GDL is approximately the same as the resistance to transverse water flow.

(v) The resistance to water flow between the GDL surface and a smooth solid surface is 10 times less than the resistance to water flow through the GDL.

(vi) Water from areas >10 cm^2 may be focused by liquid penetration to flow through a single 100 µm transverse pore of the GDL.

(vii) The collection of water through a flow directing pore network as a method to improve water management was described.

Acknowledgements

This material is based upon work supported by National Science Foundation Grant No. 0903661 "Nanotechnology for Clean Energy IGERT."

References

[1] P. Cheung, J. D. Fairweather, D. T. Schwartz, *J. Power Sources* **2009**, *187*, 487.

[2] J. D. Fairweather, P. Cheung, D. T. Schwartz, *J. Power Sources* **2010**, *195*, 787.

[3] J. D. Fairweather, P. Cheung, J. St-Pierre, D. T. Schwartz, *Electrochem. Commun.* **2007**, *9*, 2340.

[4] K. G. Gallagher, R. M. Darling, T. W. Patterson, M. L. Perry, *J. Electrochem. Soc.* **2008**, *155*, B1225.

[5] J. T. Gostick, M. W. Fowler, M. A. Ioannidis, M. D. Pritzker, Y. M. Volfkovich, A. Sakars, *J. Power Sources* **2006**, *156*, 375.

[6] J. T. Gostick, M. A. Ioannidis, M. W. Fowler, M. D. Pritzker, *Electrochem. Commun.* **2008**, *10*, 1520.

[7] J. T. I. Gostick, A. Marios, M. W. Fowler, M. D. Pritzker, Characterization of the Capillary Properties of Gas Diffusion Media, in *Modeling and Diagnostics of Polymer Electrolyte Fuel Cells* (Eds.: U. Pasaogullari, C.-Y. Wang), Springer, New York, USA, **2010**.

[8] I. R. Harkness, N. Hussain, L. Smith, J. D. B. Sharman, *J. Power Sources* **2009**, *193*, 122.

[9] J. Hinebaugh, A. Bazylak, *J. Electrochem. Soc.* **2010**, *157*, B1382.

[10] T. V. Nguyen, G. Lin, H. Ohn, X. Wang, *Electrochem. Solid State Lett.* **2008**, *11*, B127.

[11] A. Z. Weber, *J. Power Sources* **2010**, *195*, 5292.

[12] M. Mathias, J. Roth, J. Fleming, W. Lehnert, Diffusion Media Materials and Characterization, in *Handbook of Fuel Cells – Fundamentals, Technology and Applications*, Vol. 3 (Eds.: W. Vielstich, H. Gasteiger, A. Lamm), John Wiley & Sons, London **2003**.

[13] D. Bevers, R. Rogers, M. vonBradke, *J. Power Sources* **1996**, *63*, 193.

[14] K. Jiao, B. Zhou, *J. Power Sources* **2007**, *169*, 296.

[15] G. Y. Lin, T. Van Nguyen, *J. Electrochem. Soc.* **2005**, *152*, A1942.

[16] B. A. McCain, A. G. Stefanopoulou, J. B. Siegel, *J. Dyn. Syst. Meas. Control-Trans. ASME* **2010**, *132*, 061303-1.

[17] G. G. Park, Y. J. Sohn, T. H. Yang, Y. G. Yoon, W. Y. Lee, C. S. Kim, *J. Power Sources* **2004**, *131*, 182.

[18] L. J. Yang, W. A. Li, X. Z. Du, Y. P. Yang, *J. Fuel Cell Sci. Technol.* **2010**, *7*.

[19] E. Gauthier, T. Hellstern, I. G. Kevrekidis, J. Benziger, *ACS Appl. Mater. Interfaces* **2012**, *4*, 761.

[20] J. Benziger, J. Nehlsen, D. Blackwell, T. Brennan, J. Itescu, *J. Membr. Sci.* **2005**, *261*, 98.

[21] E. Kimball, T. Whitaker, Y. G. Kevrekidis, J. B. Benziger, *AIChE J.* **2008**, *54*, 1313.

[22] J. Eller, T. Rosen, F. Marone, M. Stampanoni, A. Wokaun, F. N. Buchi, *J. Electrochem. Soc.* **2011**, *158*, B963.

[23] S. Litster, D. Sinton, N. Djilali, *J. Power Sources* **2006**, *154*, 95.

[24] Z. J. Lu, M. M. Daino, C. Rath, S. G. Kandlikar, *Int. J. Hydrogen Energy* **2010**, *35*, 4222.

[25] S. Park, B. N. Popov, *Electrochim. Acta* **2009**, *54*, 3473.

[26] S. Park, B. N. Popov, *Fuel* **2011**, *90*, 436.

[27] S. Park, B. N. Popov, *Fuel* **2009**, *88*, 2068.

[28] Z. Fishman, A. Bazylak, *J. Electrochem. Soc.* **2011**, *158*, B841.

[29] J. Lobato, P. Canizares, M. A. Rodrigo, C. Ruiz-Lopez, J. J. Linares, *J. Appl. Electrochem.* **2008**, *38*, 793.

[30] J. H. Nam, K. J. Lee, G. S. Hwang, C. J. Kim, M. Kaviany, *Int. J. Heat Mass Transfer* **2009**, *52*, 2779.

[31] H. K. Atiyeh, K. Karan, B. Peppley, A. Phoenix, E. Halliop, J. Pharoah, *J. Power Sources* **2007**, *170*, 111.

[32] K. Karan, H. Atiyeh, A. Phoenix, E. Halliop, J. Pharoah, B. Peppley, *Electrochem. Solid State Lett.* **2007**, *10*, B34.
[33] A. Z. Weber, J. Newman, *J. Electrochem. Soc.* **2005**, *152*, A677.
[34] Z. Fishman, A. Bazylak, *J. Electrochem. Soc.* **2011**, *158*, B846.
[35] K. J. Lee, J. H. Kang, J. H. Nam, C. J. Kim, *J. Power Sources* **2010**, *195*, 3508.
[36] D. Gerteisen, T. Heilmann, C. Ziegler, *J. Power Sources* **2008**, *177*, 348.
[37] E. E. Kimball, J. B. Benziger, Y. G. Kevrekidis, *Fuel Cells* **2010**, *10*, 530.
[38] J. P. Feser, A. K. Prasad, S. G. Advani, *J. Power Sources* **2006**, *162*, 1226.
[39] E. F. Medici, J. S. Allen, *J. Power Sources* **2009**, *191*, 417.
[40] E. F. Medici, J. S. Allen, *J. Electrochem. Soc.* **2010**, *157*, B1505.
[41] V. Gurau, M. J. Bluemle, E. S. De Castro, Y. M. Tsou, J. A. Mann, T. A. Zawodzinski, *J. Power Sources* **2006**, *160*, 1156.
[42] D. L. Wood, C. Rulison, R. L. Borup, *J. Electrochem. Soc.* **2010**, *157*, B195.
[43] A. Theodorakakos, T. Ous, A. Gavaises, J. M. Nouri, N. Nikolopoulos, H. Yanagihara, *J. Colloid Interface Sci.* **2006**, *300*, 673.
[44] E. Gauthier, T. Hellstern, I. G. Kevrekidis, J. Benziger, *ACS Appl. Mater. Interfaces* **2012**, *4*, 761.
[45] P. K. Das, A. Grippin, A. Kwong, A. Z. Weber, *J. Electrochem. Soc.* **2012**, *159*, B489.
[46] R. B. Bird, W. E. Stewart, E. N. Lightfoot, *Transport Phenomena*, Rev. 2nd Edn., J. Wiley, New York **2007**.
[47] F. Galembeck, *J. Polym. Sci., Part C: Polym. Lett.* **1977**, *15*, 107.
[48] D. W. Dwight, W. M. Riggs, *Abstracts Pap. Am. Chem. Soc.* **1973**, 66.
[49] B. A. McCain, A. G. Stefanopoulou, I. V. Kolmanovsky, *IEEE Trans. Control Syst. Technol.* **2009**, *17*, 1055.
[50] V. Mishra, F. Yang, R. Pitchumani, *J. Fuel Cell Sci. Technol.* **2004**, *1*, 2.
[51] T. H. Zhou, H. T. Liu, *J. Power Sources* **2006**, *161*, 444.

